

Vapor Deposition of Perovskite Precursor PbI₂ on Au and Graphite

Benjamin Ecker, Ke Wang, Yongli Gao

University of Rochester, Rochester, NY 14627-0171, USA

Abstract: The energy level alignment that occurs at the interfaces in planar-hetero structured perovskite photovoltaic devices strongly influences the charge transport across the interface, and thus plays a crucial role in overall device performance. To directly observe the energy level alignment requires pristine homogeneous surfaces that are free of contamination including adventitious carbon. Co-evaporation offers the ability to grow perovskite thin films in-situ, and the method involves thermally evaporating the perovskite precursors such as PbI2 and CH3NH3I. Early reports have shown that the perovskite film formation and stoichiometry are problematic at ultralow coverages. In particular, it was reported that there was excessive PbI2 and a deficiency in CH3NH3I. Using photoemission spectroscopy, we investigated the perovskite precursor PbI2 on gold and highly oriented pyrolytic graphite (HOPG) surfaces. Results show that the nature of the surface and the deposition conditions can strongly influence the film formation. Excessive iodine observed in the initial evaporation stages appears to be substrate dependent, and this may influence the overall energy level alignment.

INTRODUCTION:

Solar cells created with hybrid organic-inorganic halide perovskites have rapidly developed with power conversion efficiencies growing from 3.8% [1] in 2009 to 25.2% [2] in 2019, and will remain the focus of considerable research efforts for the foreseeable future. Even with the remarkable improvements over the past decade, the underlying energy level alignment throughout the device has not been thoroughly investigated and optimized despite the role alignment plays in achieving high open-circuit voltages and device efficiencies. Photoemission spectroscopy remain the leading method to directly observe the electronic structure at interfaces due to the technique's surface sensitivity. Several such investigations [3-10] have examined energetic alignment of relevant device interfaces by depositing transport layers on top of a thick perovskite film, and some have shown deviations from the commonly assumed flat band and vacuum level alignment conditions. These deviations were usually attributed to the formation of an interface dipole

or a chemical reaction between the layers, and it was broadly speculated to hinder the charge separation in and extraction from the perovskite layer in a real device.

Others have opted to meticulously investigate the perovskite interface by growing in-situ the perovskite film with vapor deposited methods such as co-evaporation, and these detailed reports increasingly showed that the perovskite film growth and interfaces with it are indeed problematic. In 2016, Zhou [11] and Xu [12] both reported an initially lead iodide (PbI₂) rich interface on various substrates with the co-evaporated perovskite films, and saw the formation of a significant interface dipole with some minor band bending. Then later Olthof and Meerholz [13] reported the formation of an initial induction region which was required to passivate the substrate before a stoichiometric perovskite film formed, and that the thickness of the induction region depended "strongly on the nature of the substrate." These reports showed that at low evaporation coverages, the deposited films had significant deviations that could hinder the perovskite device performance and should certainly be investigated and optimized. A number of reports have focused entirely on investigating methylammonium iodide (MAI), and have reported some anomalous behavior [14,15] of MAI during evaporation including high vapor pressures, low sticking coefficients, perovskite film thicknesses independent on the MAI flux, and thermal decomposition. Recently, Borchert [16] reported that some of these behavioural problems during evaporation were related to impurities in the MAI created during the material synthesis.

While a great deal of discussion has focused on the MAI, the PbI₂ evaporation and its potential influence on the perovskite film formation and subsequent interfaces has not been closely examined and certainly not thoroughly investigated. A number of the two step synthesis methods for perovskite involve initially depositing a PbI₂ layer either by solution or vapor deposition methods, followed by exposure to the organic cations to transform into a perovskite film [17]. The PbI₂ deposition and film formation is also pertinent to investigate as vapor deposited PbI₂ flakes have recently attracted considerable attention for highly sensitive, flexible, and low temperature deposited photodetectors [18-20], and for their use in combination with other two dimensional materials such as MoS₂, WS₂, WSe₂ in various heterostructures [21,22]. Here we report an investigation into the deposition of the perovskite precursor PbI₂ by thermal evaporation onto clean gold (Au) and highly oriented pyrolytic graphite (HOPG) surfaces. These substrates were chosen, as the metallic Au surface and the covalently bonded HOPG surfaces were expected to interact differently with the ionic PbI₂ material.

EXPERIMENTAL DETAILS

The pristine Au surface was created with Ar^+ sputtering to remove surface contamination from a Au-coated-Si substrate, and the fresh HOPG surface was created by in-situ exfoliation via scotch tape. To directly examine the interface, a sequential series of PbI_2 depositions and photoemission measurements were performed on each substrate. The PbI_2 was deposited in a separate evaporation chamber with a dedicated pumping system, and the rate was stabilized to 1Å/min and monitored with a quartz crystal microbalance. After reaching the desired thickness, the sample was transferred to the analysis chamber for ultraviolet and x-ray photoemission measurements (UPS and XPS, respectively). The analysis chamber was a modified VG ESCA Lab system equipped with a helium discharge lamp and twin anode x-ray source. After the sequence of evaporations and measurements, the evaporation chamber's atmosphere was examined with a residual gas analyser (Extorr Inc, XT300M) which uses a quadrupole for mass spectrometry (see the supporting material for additional information regarding the experimental details).

RESULTS AND DISCUSSIONS

Ultraviolet Photoemission Spectroscopy

The UPS stack plots for secondary cut-off and valence band region (highest occupied molecular orbitals) for PbI_2 deposition on the Au and HOPG surfaces can be seen in Fig. 1 (a) and (b), respectively. The zero-point binding energy in the plots represents the fermi level position measured of the Ar sputtered clean Au surface. The presence of the Au 5d intrinsic surface states seen the in first scan of valence band region in Fig. 1(a) are an indication of an atomically clean surface.

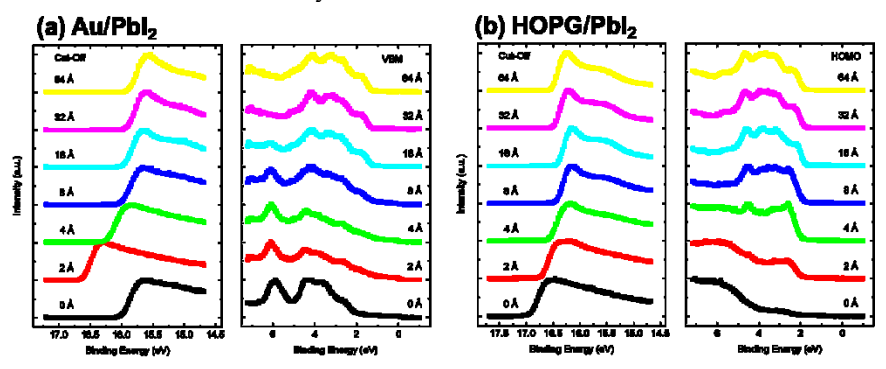


Figure 1. The UPS stack plots for the secondary cut-off and valence band regions for increasing depositions of PbI₂ onto a) Au and b) HOPG surfaces, respectively.

Upon deposition of 2 Å of PbI_2 to the Au surface seen in Fig. 1(a), a strong initial shift of 0.64 eV to higher binding energies in the cut-off can be seen resulting in the work function changing from 5.35 eV at 0 Å to 4.71 eV at 2 Å. The movement of the cut-off then rapidly pulls back and appeared to saturate at 8 Å to 5.45 eV, which is very close to the reported value for interlayer spacing in PbI_2 platelets at 7.03 Å [23]. This shift may have been the result of the pushback effect (also referred to as the cushion effect) that is often seen at the metal/organic interfaces, but it might also be an indication of the formation of an interface dipole layer. Meanwhile in the valence band maximum region, there is a rapid reduction in the Au 5d surface states and the formation of the PbI_2 spectral features upon its deposition. It is difficult to discern the exact valence band position at low coverages, as the Au fermi level is clearly observable up to and including 8 Å. Afterwards, the valence band position appeared to saturate at 1.31 eV making the PbI_2 deposition slightly n-type for the material which has been reported to have a bandgap of about 2.3 eV [24].

The UPS stack plots for the PbI₂ deposition onto the HOPG surface are shown in Fig. 1(b), and the behaviour the evolution of the cut-off and valence band region are distinctly different than the Au surface. There is a much smaller shift of approximately 0.18 eV in the cut-off to lower binding energy going from 0 Å to 2 Å, corresponding to a work function change of 4.44 eV to 4.62 eV. The cut-off continues to gradually shift to lower binding energy before saturating again around 8 Å, and the surface has a work function of approximately 4.85 eV. While in the valence band region, the PbI₂ develops much more rapidly and clearly even at a deposition of 2 Å. Though this discrepancy in behaviour may just be more evident due to HOPG's low density of states near the fermi region compared to that of the Au surface. The valence band position settles very quickly to 1.85 eV, making the deposition clearly n-type, even more so that on the Au surface. Additionally, a feature clearly develops at about 2.5 eV below the fermi level and continues

to grow until 8Å, after which it then diminishes with further depositions. This growth followed by attenuation behavior suggest that an extrinsic surface state had formed between the HOPG and PbI₂, This state is categorically different than the intrinsic surface state seen on the pristine Au surface, as it was not due to individual HOPG or PbI₂ surfaces, but instead due to the interface. A similar state was not observed in the Au/PbI₂ interface.

X-ray Photoemission Spectroscopy

Similar XPS stack plots for the substrate (Au 4f or C1s), and Pb 4f and I 3d_{5/2} core level for the PbI₂ deposition on Au and HOPG can be seen in the supplementary materials. By closely examining the relative intensity change for the substrate core levels, the PbI₂ growth mode can be determined by plotting the logarithm of the intensity versus deposition coverage, and this is plotted in Fig. 2(a). For both substrates, the core levels intensity decays linearly on the logarithmic scale (exponentially on linear), suggesting that on both substrates the PbI₂ grows by Frank van der Merwe (or layer by layer) type growth. This suggests that the interaction between the PbI₂ and the substrate is balanced with the PbI₂-PbI₂ interaction, and that the deposition by Frank van der Merwe type growth will produce smooth films. Additionally, both substrates have an attenuation length, or the deposition coverage where the intensity is 1/e the bare substrates intensity, is very close to 20 Å. More precisely, the attenuation length is 23 Å and 17 Å for the Au and HOPG surface coverages, respectively. These values are very close to the expected minimum value of the universal inelastic mean free path curve.

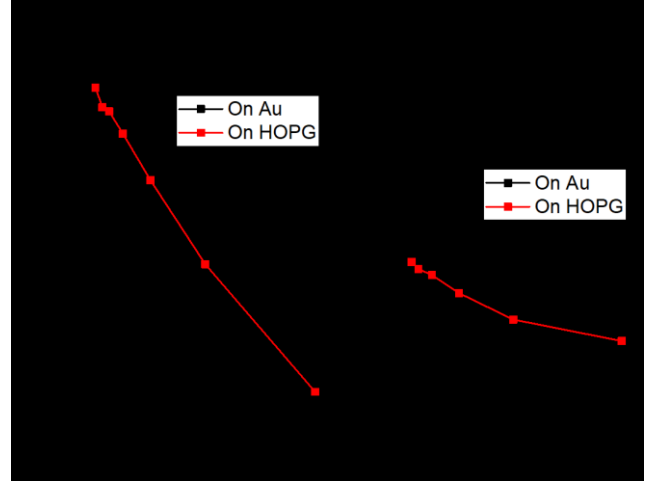


Figure 2. a) The Au $4f_{7/2}$ and C 1s core level's intensity attenuation from increasing deposition of PbI₂ which were observed from the series of XPS measurements. The intersection with the dashed line at minus one represents the expected attenuation length. b) The relative stoichiometric ratio of iodine to lead measured by XPS changes with increasing depositions of PbI₂. The dashed line here represents the expected ratio 2-to-1 for PbI₂.

When we then examined the relative intensity changes of the overlayer components by looking at the atomic ratio of I to Pb plotted here in Fig. 2(b), we saw significant stoichiometric variations from the expected ratio of 2. On the Au surface, the initial ratio was greater than 7 at 2 Å deposition, and then the ratio then appeared to exponentially decay on the Au surface with increasing deposition. This exponential behaviour was very suggestive of some sort of interfacial layer of iodine, as the signal from this interface layer would be then be attenuated by the increasing depositions. Even at the final deposition of 64Å, the I to Pb ratio did not reach the expected value of 2. This

interfacial iodine on the Au surface was further confirmed by modelling the core levels of the substrates and overlayer, and the model is briefly described in the supplemental materials. The model also showed the expected growth or attenuation for all other core levels with no additional interface or surface contributions. Similarly, the I to Pb ratio on the HOPG surface was initially high and was slightly greater than 4. Instead of exponential behaviour, the ratio followed a more linear-like decrease suggesting a non-stoichiometric deposition rather than an interface layer of iodine.

This result was somewhat surprising, as there have not been previous reports suggesting problems with PbI₂ deposition by thermal evaporation. Though, similar non-stoichiometric behaviour and excess iodine was also seen in the previous reports for CH₃NH₃PbI₃ depositions by co-evaporation where the I to Pb ratio was expected to be 3 to 1 [11-13]. This result in particular suggests that some of the problems with the initial deposition of the perovskite by co-evaporation may be due to the excess iodine located at the interface with the substrate, and not purely due to the issues with MAI evaporations.

Excess iodine

After analysis, we really wanted to explore the source of the extra iodine, and so, fresh Au and HOPG substrates were placed inside the evaporation chamber. The chamber had no on-going thermal evaporations and had no previous evaporations for over 24 hrs, so that the chamber was essentially at equilibrium. After 30 minutes, the sample were insitu transferred to the analysis chamber and measured, and the I 3d_{5/2} core level for post and pre exposure can be seen in Fig. 3 (a). For the Au substrate, the various collected measurements for the work function, valence band region, and the Au and I core levels looked remarkably similar to the 2 Å PbI₂ deposition seen previously. This suggested that there was an established contamination environment inside the evaporation chamber that was ever present and was responsible for at least some of the excess I seen before on Au. However, for the HOPG substrate, very little iodine was observed, suggesting at the very least that the HOPG surface was resistant to the evaporation chamber's contamination.

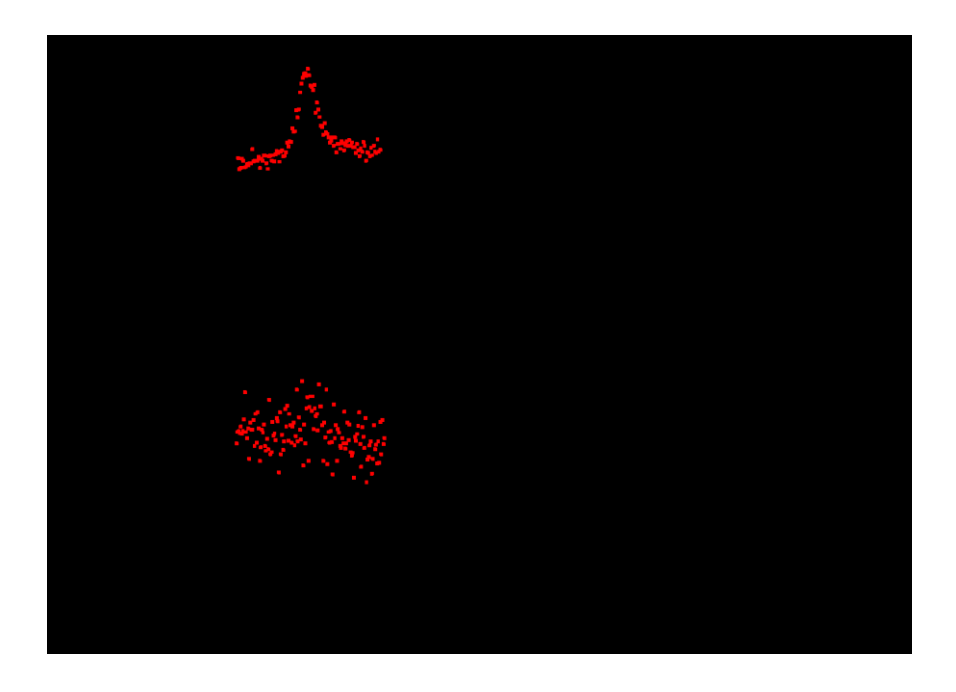


Figure 3. a) The I $3d_{5/2}$ core level on Au and HOPG surfaces before and after after being placed inside the "cold" evaporation chamber. b) A mass sweep scan from the residual gas analyzer that shows partial pressures at a given mass per charge ratios.

A residual gas analyser revealed that the iodine likely was present in the form of HI and in a trace amount CH_3I , suggesting this iodine was coming from previous evaporations of MAI. Surprisingly though, no molecular iodide (I_2) was ever observed. A sample mass sweep from the RGA of the "cold" chamber can be seen in Fig. 3 (b). This chamber contamination in the form of HI readily formed even after venting and purging the system. This suggest it is an extremely pervasive contamination issue for vacuum systems, as it is not practical to physically open up a vacuum deposition system and clean after every evaporation. It is not clear whether other perovskite cations would also create a similar contamination issues when thermally evaporated.

CONCLUSIONS

Here we have presented our photoemission investigation into PbI_2 deposition onto Au and HOPG surfaces. Our report shows that the while the PbI_2 rapidly developed electronically on both surfaces by thermal evaporation, that it also deposited non-stoichiometrically with excess iodine particularly at ultra-low coverages. Further investigations into the evaporation chamber revealed that some of the excess iodine could be attributed to residual contamination from previous perovskite growths in the evaporation chamber. Fresh Au substrates developed a significant iodine signal when placed into the "cold" chamber with no on-going evaporations, while the HOPG substrates did not. A residual gas analyser revealed that the iodine was likely present in the form of HI, suggesting this iodine came from previous MAI evaporations. This chamber contamination readily formed even after venting the system, and quickly returned after cleanings. Not surprisingly, HI is an extremely pervasive contamination issue for vacuum

systems, and it is not practical to physically open up and clean a vacuum deposition system after every evaporation. It would be pertinent to investigate whether the other common perovskite precursors produce similar contamination issues when evaporated and what influence it may have on the perovskite film growth.

UPS measurements showed that even with the contamination, the work function and valence band regions of the interfaces with PbI2 readily developed and saturated within 16Å of deposition, and that the deposited films were measured to be n-type on both substrates. Though the chamber contamination certainly complicates the previous binding energy shift's interpretations, particularly for the Au/PbI₂ interface, as the shifts were from partially to fully due to the HI contaminate. The behaviour of the attenuation of the core levels Au 4f_{7/2} and C 1s, for both the Au and HOPG surfaces, seen by the XPS measurements suggested that the PbI₂ grew by Frank van der Merwe type growth (or layer by layer). However, the XPS measurements also revealed that the PbI₂ was not depositing stoichiometrically on both surfaces. By modelling the I 3d_{5/2} core level's growth, it was clear that an interfacial layer of iodine had formed on the Au surface, and this iodine was at least partially from the chamber's HI atmosphere. The model also suggested that the iodine layer was also absent from the HOPG surface, which on one hand agrees with the "cold" chamber tests, but on the other it does not explain the nonstoichiometric deposition seen at the HOPG/PbI₂ interface. Overall, these results suggest that at least some of the problems with the initial deposition of perovskite by coevaporation may be related to issues with PbI₂ deposition, and not purely due to issues with MAI evaporation.

References:

- 1. A. Kojima, K. Teshima, Y. Shirai and T. Miyasaka, J Am Chem Soc 131 (17), 6050 (2009). NREL, 2019.
- 3. P. Schulz, E. Edri, S. Kirmayer, G. Hodes, D. Cahen and A. Kahn, Energy Environ. Sci. 7 (4), 1377 (2014).
- M. F. Lo, Z. Q. Guan, T. W. Ng, C. Y. Chan and C. S. Lee, Adv. Funct. Mater. 25 (8), 4. 1213 (2015).
- 5.
- 6.
- 7.
- 1213 (2015).
 P. Schulz, L. L. Whittaker-Brooks, B. A. MacLeod, D. C. Olson, Y. L. Loo and A. Kahn, Adv. Mater. Interfaces **2** (7), 1400532 (2015).
 C. G. Wang, X. L. Liu, C. C. Wang, Z. G. Xiao, C. Bi, Y. C. Shao, J. S. Huang and Y. L. Gao, J. Vac. Sci. Technol. B **33** (3), 032401 (2015).
 Q. K. Wang, R. B. Wang, P. F. Shen, C. Li, Y. Q. Li, L. J. Liu, S. Duhm and J. X. Tang, Adv. Mater. Interfaces **2** (3), 1400528 (2015).
 E. S. Thibau, A. Llanos and Z. H. Lu, Appl. Phys. Lett. **108** (2), 021602 (2016).
 X. Liu, C. Wang, L. Lyu, C. Wang, Z. Xiao, C. Bi, J. Huang and Y. Gao, Phys Chem Chem Phys **17** (2), 896 (2015).
 P. Liu, X. L. Liu, L. Lyu, H. P. Xie, H. Zhang, D. M. Niu, H. Huang, C. Bi, Z. G. Xiao, J. S. Huang and Y. L. Gao, Appl. Phys. Lett. **106** (19), 193903 (2015).
 X. Zhou, X. Li, Y. Liu, F. Huang and D. Zhong, Appl. Phys. Lett. **108** (12), 121601 (2016).
- 10.
- 11.
- (2010).
 H. Xu, Y. Wu, J. Cui, C. Ni, F. Xu, J. Cai, F. Hong, Z. Fang, W. Wang, J. Zhu, L. Wang, R. Xu and F. Xu, Phys Chem Chem Phys 18 (27), 18607 (2016).
 S. Olthof and K. Meerholz, Sci Rep 7, 40267 (2017).
 M. J. Bækbo, O. Hansen, I. Chorkendorff and P. C. K. Vesborg, RSC Adv. 8 (52), 29899 12.
- 14. (2018).
- A. Llanos, E. S. Thibau and Z. H. Lu, J Vac Sci Technol A 34 (6), 060601 (2016). 15.
- J. Borchert, I. Levchuk, L. C. Snoek, M. U. Rothmann, R. Haver, H. J. Snaith, C. J. Brabec, L. M. Herz and M. B. Johnston, ACS Appl. Mater. Interfaces 11 (32), 28851 16.
- 17.
- 18.
- K. Liang, D. B. Mitzi and M. T. Prikas, Chem. Mater. **10** (1), 403 (1998). Y. Wang, L. Gan, J. Chen, R. Yang and T. Zhai, Sci. Bull. **62** (24), 1654 (2017). J. Zhang, Y. Huang, Z. Tan, T. Li, Y. Zhang, K. Jia, L. Lin, L. Sun, X. Chen, Z. Li, C. Tan, J. Zhang, L. Zheng, Y. Wu, B. Deng, Z. Chen, Z. Liu and H. Peng, Adv Mater, **20** 1803194 (2018). 19.

- 20.
- J. Y. Zhang, T. Song, Z. J. Zhang, K. Ding, F. Huang and B. Q. Sun, J. Mater. Chem. C 3 (17), 4402 (2015).
 Y. Sun, Z. Zhou, Z. Huang, J. Wu, L. Zhou, Y. Cheng, J. Liu, C. Zhu, M. Yu, P. Yu, W. Zhu, Y. Liu, J. Zhou, B. Liu, H. Xie, Y. Cao, H. Li, X. Wang, K. Liu, X. Wang, J. Wang, L. Wang and W. Huang, Adv Mater 31 (17), 1806562 (2019).
 W. Zheng, B. Zheng, C. Yan, Y. Liu, X. Sun, Z. Qi, T. Yang, Y. Jiang, W. Huang, P. Fan, F. Jiang, W. Ji, X. Wang and A. Pan, Adv Sci 6 (7), 1802204 (2019).
 X. Liu, S. T. Ha, Q. Zhang, M. de la Mata, C. Magen, J. Arbiol, T. C. Sum and Q. Xiong, ACS Nano 9 (1), 687 (2015).
 D. S. Ahlawat, Mod. Phys. Lett. B 26 (16), 1250098 (2012). 21.
- 22.
- 23.
- 24.